Vibrational relaxation of carbon dioxide in state-to-state and multi-temperature approaches

O. Kunova,[1,*] A. Kosareva,[†] E. Kustova,[‡] and E. Nagnibeda[§]
Saint-Petersburg State University, Department of Mathematics and Mechanics, 7/9 Universitetskaya nab., St. Petersburg 199034, Russia

(Received 3 June 2020; accepted 5 November 2020; published 2 December 2020)

Vibrational relaxation of single-component carbon dioxide is studied using the full and reduced state-to-state models and two multi-temperature approaches. The full kinetic scheme including all vibrational states and different kinds of vibrational energy transitions within and between CO_2 modes is proposed and implemented to the 0-D code for spatially homogeneous relaxation. Contributions of various energy transitions are evaluated, and dominating relaxation mechanisms are identified for two generic test cases corresponding to compression (excitation) and expansion (deactivation) regimes. It is shown that the main relaxation channels are vibrational-translation (VT) transitions in the symmetric and bending modes and two intermode vibrational-vibrational (VV) exchanges. Reduced-order models are assessed by comparisons with the results of full state-to-state simulations. The commonly used two-temperature model with the single vibrational temperature fails to describe the relaxation for all considered initial conditions. The three-temperature model provides a good agreement with the state-to-state simulations for the excitation regime, but yields a considerable discrepancy for the deactivation mode. The sources of the discrepancies are detected and several ways for the improvement of numerically efficient multi-temperature models are proposed.

DOI: 10.1103/PhysRevFluids.5.123401

I. INTRODUCTION

Carbon dioxide is a key species for many fundamental and applied problems, including Mars entry, laser technologies, Earth environmental issues, and greenhouse gas conversion into fuels. Studies of nonequilibrium CO_2 kinetics are carried out by many scientific groups on the basis of state-to-state [1–12], multi-temperature [13–18], coarse-graining [19], and drift-diffusion [10] approaches. State-resolved models give a deep insight into the physics of vibrationally excited states, but are hardly applicable in engineering problems due to their high computational costs, especially in polyatomic gases. Thus, two serious problems arise when CO_2 vibrational relaxation is studied in the frame of the state-to-state approximation. First, in this approach, the gas dynamic equations should be coupled to several thousands of equations for populations of each level of three CO_2 vibrational modes (symmetric, bending, and asymmetric). Second, the energy production terms in these equations contain hundreds of thousands of rate coefficients for different processes: vibrational-translational (VT) energy transitions within three CO_2 modes, and vibrational-vibrational (VV) energy exchanges between different states of vibrational modes.

*o.kunova@spbu.ru.
†kos-hellen@yandex.ru.
‡e.kustova@spbu.ru.
§e_nagnibeda@mail.ru.

Recently, as a first step towards numerical application of the state-to-state approach, a numerical scheme for the calculation of state-dependent CO_2 rate coefficients was proposed in [20] on the basis of parallel computations. However, its implementation to computational fluid dynamics (CFD) still remains a challenge, and reduced-order models are of crucial importance.

Coarse-graining methods [19,21], although providing an efficient technique for inviscid flow simulations taking into account strongly nonequilibrium effects, are still unable to describe the transport coefficients for energy bins; therefore, their application for viscous flow simulations is questionable. Two-temperature models commonly used in CFD [13] are rather efficient but, in the case of CO_2, cannot take into account various vibrational modes and different rates of vibrational energy exchange between modes [18]. More realistic multi-temperature models that take into account energy exchange between asymmetric and coupled symmetric-bending CO_2 modes were developed in [14,16] within the framework of the generalized Chapman-Enskog method. The models provide algorithms for evaluation of the transport terms and can be used in both inviscid and viscous flow simulations; they were applied in [22] for simulations of shock heated CO_2 flows and in [15,23] for two-dimensional (2D) modeling of flows around the Mars sample return orbiter, cone, and sphere. One of the limitations of these implementations is that the energy production terms are written in the simplified Landau-Teller form, which is not applicable for intermode vibrational energy exchange. Moreover, contrary to air mixtures, no comparison of state-to-state and multi-temperature simulations was carried out in nonequilibrium CO_2 flows, except one particular case studied in [17]. Thus, the range of applicability of multi-temperature models was not assessed until the present time. The same problem holds for the reduced state-resolved kinetic schemes used in the CFD [2,6,8].

State-to-state simulations provide a powerful tool for the assessment of reduced models when reliable experimental data are not available. Some steps in such assessments are done in [3,4,11,12], where thorough studies of a one-dimensional CO_2 flow along the stagnation line were carried out within the full and reduced state-to-state approaches; the surface heat flux was compared with experiments [24,25] and a good agreement was shown. Nevertheless, the above studies have several limitations: due to high computational efforts, it was not possible to take into account all CO_2 vibrational states, and the vibrational ladder was cut at the energy 3 eV, which is considerably less than the dissociation energy. For the same reason, intramode VV transitions were not taken into account. Moreover, only a few specific test cases were studied, all of them corresponding to the stagnation line flows; other conditions were not considered. In order to assess the various models under different conditions, the most efficient way is to use 0-D thermal bath simulations or a spatially homogeneous problem. By varying the initial gas temperature, pressure, vibrational temperatures, and mixture composition, one can reproduce arbitrary deviations from equilibrium corresponding to different real gas flows without huge computational efforts.

The objectives of the present study are (1) further development and implementation of the full kinetic scheme for modeling CO_2 vibrational kinetics in the state-to-state approach, (2) identifying key mechanisms of vibrational relaxation in the single-component CO_2 under various initial conditions, (3) assessment of the two-temperature and three-temperature models of vibrational relaxation and reduced state-to-state kinetic schemes, and (4) evaluation of the contributions of different vibrational energy transitions to the relaxation processes. Since the main focus is on the vibrational kinetics, we do not discuss in this study vibrational-chemical coupling and consider a single-component carbon dioxide.

The paper is organized as follows. First, in Sec. II, we develop the extended state-to-state kinetic scheme including all known mechanisms of vibrational energy transitions, revise the expressions for the rate coefficients of multi-quantum transitions, and describe an improved algorithm for the numerical implementation of the state-to-state model. Then, in Sec. III, we review the two- and three-temperature models and discuss the issues with the calculation of the production terms. In Sec. IV, we show the comparison of the results for the 0-D spatially homogeneous relaxation using various kinetic schemes and models, discuss key relaxation mechanisms under different initial

conditions, and assess the reduced state-to-state kinetic schemes. The main results are summarized in the Conclusions in Sec. V.

II. STATE-TO-STATE DESCRIPTION

Implementation of the state-to-state model is necessary under conditions of strong deviations from thermal equilibrium, when the characteristic times of all vibrational energy transitions are comparable to the characteristic fluid-dynamic time,

$$\tau_{tr} < \tau_{\text{rot}} \ll \tau_{\text{vibr}} \sim \theta, \tag{1}$$

where τ_{tr}, τ_{rot}, and τ_{vibr} are, respectively, the relaxation times for the translational, rotational, and vibrational degrees of freedom, and θ is the macroscopic timescale. Different kinds of vibrational energy transitions are discussed below. In this study, we consider the single-component gas and, therefore, do not take into account chemical reactions.

A. Governing equations

The vibrational relaxation of a spatially homogeneous CO_2 gas is described by the set of equations

$$\frac{dn_{i_1,i_2,i_3}}{dt} = \sum_{\gamma} R^{\gamma}_{i_1,i_2,i_3}, \quad i_m = 0, \ldots, l_m, \quad m = 1, 2, 3, \tag{2}$$

$$U = E_{tr} + E_{\text{rot}} + E_{\text{vibr}} = \text{const}. \tag{3}$$

Here, n_{i_1,i_2,i_3} is the population of the (i_1, i_2, i_3) vibrational state, quantum numbers i_1, i_2, i_3 correspond to the symmetric, doubly degenerated bending, and asymmetric vibrations of a CO_2 molecule. The production terms $R^{\gamma}_{i_1,i_2,i_3}$ describe the variation of the level populations as a result of vibrational energy transitions through the process γ, l_m is the maximum vibrational level number in mth mode, and U is the total energy per unit mass expressed as a sum of translational, rotational, and vibrational energies.

Under the assumption of the Maxwell velocity distribution of particles, the translational energy has the form

$$\rho E_{tr} = \tfrac{3}{2} n k_B T. \tag{4}$$

The CO_2 molecule is linear, and therefore the rotational energy of the gas for the rigid rotator model can be written in the form

$$\rho E_{\text{rot}} = n k_B T. \tag{5}$$

The vibrational energy of the gas is described as follows:

$$\rho E_{\text{vibr}} = \sum_{i_1,i_2,i_3} n_{i_1,i_2,i_3} \varepsilon_{i_1,i_2,i_3}. \tag{6}$$

In Eqs. (4)–(6), ρ is the gas density, n is the total number density, k_B is the Boltzmann constant, T is the gas temperature, and $\varepsilon_{i_1,i_2,i_3}$ is the vibrational energy of a molecule at the (i_1, i_2, i_3)-th vibrational state. The vibrational energy of CO_2 molecules was described on the basis of the harmonic and anharmonic oscillator models [26] with $l_{1/2/3} = 30/61/17$ and $l_{1/2/3} = 30/62/19$, respectively. When calculating the partition functions and specific vibrational energy, we take into account the coupled states below the dissociation threshold D; therefore, we put the restriction $\varepsilon_{i_1,i_2,i_3} < D$ in summations over vibrational states. It is worth noting that in the present study, we assume separate normal modes up to the dissociation threshold instead of introducing the quasicontinuum of the states; strong mode interaction is simulated by accounting for all kinds of intermode vibrational transitions.

B. Set of kinetic processes

The complex structure of the CO_2 molecule leads to a large number of different exchanges of vibrational energy. Below, the main groups of exchange processes and the corresponding relaxation terms are presented. The first group includes VT_m *energy exchanges* between the translational energy and vibrational energy of the mth CO_2 mode ($m = 1, 2, 3$) as a result of the collision of two CO_2 molecules, of which the vibrational energy of one does not change. The production terms in Eqs. (2) for these processes have the following form:

(i) $VT_1 : CO_2(i_1, i_2, i_3) + CO_2 \leftrightarrow CO_2(i_1 \pm 1, i_2, i_3) + CO_2$

$$R^{VT_1}_{i_1,i_2,i_3} = n\big(n_{i_1+1,i_2,i_3} k_{i_1+1,i_1} + n_{i_1-1,i_2,i_3} k_{i_1-1,i_1} - n_{i_1,i_2,i_3}\big[k_{i_1,i_1+1} + k_{i_1,i_1-1}\big]\big), \tag{7}$$

(ii) $VT_2 : CO_2(i_1, i_2, i_3) + CO_2 \leftrightarrow CO_2(i_1, i_2 \pm 1, i_3) + CO_2$

$$R^{VT_2}_{i_1,i_2,i_3} = n\big(n_{i_1,i_2+1,i_3} k_{i_2+1,i_2} + n_{i_1,i_2-1,i_3} k_{i_2-1,i_2} - n_{i_1,i_2,i_3}\big[k_{i_2,i_2+1} + k_{i_2,i_2-1}\big]\big), \tag{8}$$

(iii) $VT_3 : CO_2(i_1, i_2, i_3) + CO_2 \leftrightarrow CO_2(i_1, i_2, i_3 \pm 1) + CO_2$

$$R^{VT_3}_{i_1,i_2,i_3} = n\big(n_{i_1,i_2,i_3+1} k_{i_3+1,i_3} + n_{i_1,i_2,i_3-1} k_{i_3-1,i_3} - n_{i_1,i_2,i_3}\big[k_{i_3,i_3+1} + k_{i_3,i_3-1}\big]\big). \tag{9}$$

Usually, only VT_2 transitions are taken into account in nonequilibrium flow simulations [3,5,14] since their rates are considerably higher than those of VT_1 and VT_3 exchange. We check this assumption in the following sections.

The second group incorporates multi-quantum *intermode* VV_{k-m} *exchanges* inside one molecule:

(iv) $VV_{1-2} : CO_2(i_1, i_2, i_3) + CO_2 \leftrightarrow CO_2(i_1 \pm 1, i_2 \mp 2, i_3) + CO_2$

$$\begin{aligned} R^{VV_{1-2}}_{i_1,i_2,i_3} = n\big(&n_{i_1+1,i_2-2,i_3} k_{i_1+1,i_2-2\to i_1,i_2} + n_{i_1-1,i_2+2,i_3} k_{i_1-1,i_2+2\to i_1,i_2} \\ &- n_{i_1,i_2,i_3}\big[k_{i_1,i_2\to i_1+1,i_2-2} + k_{i_1,i_2\to i_1-1,i_2+2}\big]\big), \end{aligned} \tag{10}$$

(v) $VV_{2-3} : CO_2(i_1, i_2, i_3) + CO_2 \leftrightarrow CO_2(i_1, i_2 \pm 3, i_3 \mp 1) + CO_2$

$$\begin{aligned} R^{VV_{2-3}}_{i_1,i_2,i_3} = n\big(&n_{i_1,i_2+3,i_3-1} k_{i_2+3,i_3-1\to i_2,i_3} + n_{i_1,i_2-3,i_3+1} k_{i_2-3,i_3+1\to i_2,i_3} \\ &- n_{i_1,i_2,i_3}\big[k_{i_2,i_3\to i_2+3,i_3-1} + k_{i_2,i_3\to i_2-3,i_3+1}\big]\big), \end{aligned} \tag{11}$$

(vi) $VV_{1-2-3} : CO_2(i_1, i_2, i_3) + CO_2 \leftrightarrow CO_2(i_1 \pm 1, i_2 \pm 1, i_3 \mp 1) + CO_2$

$$\begin{aligned} R^{VV_{1-2-3}}_{i_1,i_2,i_3} = n\big(&n_{i_1+1,i_2+1,i_3-1} k_{i_1+1,i_2+1,i_3-1\to i_1,i_2,i_3} + n_{i_1-1,i_2-1,i_3+1} k_{i_1-1,i_2-1,i_3+1\to i_1,i_2,i_3} \\ &- n_{i_1,i_2,i_3}\big[k_{i_1,i_2,i_3\to i_1+1,i_2+1,i_3-1} + k_{i_1,i_2,i_3\to i_1-1,i_2-1,i_3+1}\big]\big). \end{aligned} \tag{12}$$

These processes are selected based on the lowest-energy variations during the transition: $\Delta\varepsilon_{VV_{1-2}} = 10.54\ \mathrm{cm}^{-1}$, $\Delta\varepsilon_{VV_{2-3}} = 359.96\ \mathrm{cm}^{-1}$, and $\Delta\varepsilon_{VV_{1-2-3}} = 349.42\ \mathrm{cm}^{-1}$. Whereas VV_{1-2} exchange is almost resonant, in other intermode transitions, some part of the energy is transferred to the translational mode, but the energy variation is considerably less than in VT transitions (for instance, $\Delta\varepsilon_{VT_2} = 667.25\ \mathrm{cm}^{-1}$). Low-energy variation causes high probability of these energy exchanges.

The third group of processes includes *intramode* VV_m *exchanges* of vibrational quanta in each mth mode of the CO_2 molecule:

(vii) $VV_1 : CO_2(i_1, i_2, i_3) + CO_2(k_1, k_2, k_3) \leftrightarrow CO_2(i_1 \pm 1, i_2, i_3) + CO_2(k_1 \mp 1, k_2, k_3)$

$$\begin{aligned} R^{VV_1}_{i_1,i_2,i_3} = \sum_{k_1,k_2,k_3} \big(&n_{i_1+1,i_2,i_3} n_{k_1-1,k_2,k_3} k^{k_1-1,k_1}_{i_1+1,i_1} + n_{i_1-1,i_2,i_3} n_{k_1+1,k_2,k_3} k^{k_1+1,k_1}_{i_1-1,i_1} \\ &- n_{i_1,i_2,i_3} n_{k_1,k_2,k_3}\big[k^{k_1,k_1-1}_{i_1,i_1+1} + k^{k_1,k_1+1}_{i_1,i_1-1}\big]\big), \end{aligned} \tag{13}$$

(viii) $VV_2 : CO_2(i_1, i_2, i_3) + CO_2(k_1, k_2, k_3) \leftrightarrow CO_2(i_1, i_2 \pm 1, i_3) + CO_2(k_1, k_2 \mp 1, k_3)$

$$R^{VV_2}_{i_1,i_2,i_3} = \sum_{k_1,k_2,k_3} \left(n_{i_1,i_2+1,i_3} n_{k_1,k_2-1,k_3} k^{k_2-1,k_2}_{i_2+1,i_2} + n_{i_1,i_2-1,i_3} n_{k_1,k_2+1,k_3} k^{k_2+1,k_2}_{i_2-1,i_2} \right.$$
$$\left. - n_{i_1,i_2,i_3} n_{k_1,k_2,k_3} \left[k^{k_2,k_2-1}_{i_2,i_2+1} + k^{k_2,k_2+1}_{i_2,i_2-1} \right] \right), \tag{14}$$

(ix) $VV_3 : CO_2(i_1, i_2, i_3) + CO_2(k_1, k_2, k_3) \leftrightarrow CO_2(i_1, i_2, i_3 \pm 1) + CO_2(k_1, k_2, k_3 \mp 1)$

$$R^{VV_3}_{i_1,i_2,i_3} = \sum_{k_1,k_2,k_3} \left(n_{i_1,i_2,i_3+1} n_{k_1,k_2,k_3-1} k^{k_3-1,k_3}_{i_3+1,i_3} + n_{i_1,i_2,i_3-1} n_{k_1,k_2,k_3+1} k^{k_3+1,k_3}_{i_3-1,i_3} \right.$$
$$\left. - n_{i_1,i_2,i_3} n_{k_1,k_2,k_3} \left[k^{k_3,k_3-1}_{i_3,i_3+1} + k^{k_3,k_3+1}_{i_3,i_3-1} \right] \right). \tag{15}$$

Taking into account VV_m transitions in CO_2 is extremely computationally demanding. In some studies based on the reduced kinetic schemes [5], VV_3 transitions are supposed to be responsible for fast pumping of highly located states in the asymmetric mode, thus enhancing dissociation. In the present study, the role of VV_m transitions is discussed in the framework of the reduced kinetic scheme.

In Eqs. (7)–(15) above, $k_{i,i'}$, $k_{i\to i'}$, and $k^{k,k'}_{i,i'}$ are the rate coefficients of the corresponding processes.

C. Rate coefficients of vibrational energy transitions

Reliable data on the rate coefficients of vibrational energy transitions in carbon dioxide are scarce. There are experimental data on the selected transitions between the lowest states [27–30]; these data are often interpolated for the higher states using the formulas of the Schwartz-Slawsky-Herzfeld (SSH) theory [31]. However, the range of validity of experimental measurements is limited by low temperatures. One can mention a few works on the quasiclassical trajectory calculations of the rate coefficients in CO_2 [32–34]. Unfortunately, the results are obtained only for several transitions and thus cannot be used in our simulations; moreover, these works sometimes report the transitions which are not detected in experiments.

Theoretical approaches include the first-order perturbation SSH theory [31] and the forced harmonic oscillator (FHO) model [35]. Recently, the FHO model was extended for three-atomic gases [36]. However, due to the different vibrational ladders used in our study and in [36], we were not able to assess this data. Therefore, we used the most common approach based on the SSH model [31]: only single-quantum energy exchanges (as the most probable) are taken into account for VT_m and VV_m transitions.

It is interesting to note that in our previous studies [3,11,37], we used the original formulas given in [31]. And on the basis of these formulas, the contribution of VV_{2-3} transitions was found to be considerably greater than that of VV_{1-2-3}, which is not confirmed by the experimental data showing close values of the rate coefficients for these processes. Therefore, we decided to check the formulas given in [31].

First, we noticed a mismatch of the dimension in the original formula [31] for the interaction potential of two-quantum transitions. The expression should be as follows:

$$V(i_m \to i_m \pm 2) = \frac{(\alpha^* A_m)^2}{2!} \frac{\sqrt{(i_m + 1 \pm 1)(i_m \pm 1)}}{2\alpha}, \quad m = 1, 2, 3, \tag{16}$$

where $\alpha = 4\pi^2 M_m \nu_m / h$, α^* is the factor of potential function, A_m are the internal motion coefficients, i_m is the state of mth mode, and M_m and ν_m are the oscillator mass and frequency of the mth mode. An analogous relationship was given in the work [38]. Thus, the ratio between the original formula and the corrected one is

$$\frac{V^{or}}{V^{cor}} = \sqrt{4\alpha},$$

which gives a significant discrepancy in the rate coefficients.

Furthermore, we derived the expression for the three-quantum transitions potential which was missing in the original article:

$$V(i_m \to i_m \pm 3) = -\frac{(\alpha^* A_m)^3}{3!}\frac{\sqrt{(i_m + 1.5 \pm 1.5)(i_m \pm 2)(i_m \pm 1)}}{(2\alpha)^{3/2}}. \tag{17}$$

Taking into account the above corrections, we obtain the rate coefficients of VV_{2-3} and VV_{1-2-3} transitions of the same order of magnitude, which agree well with the experimental data [28].

D. Numerical implementation

As mentioned in Sec. II A, the vibrational energy of the CO_2 molecule $\varepsilon_{i_1,i_2,i_3}$ depends on the state of three coupled modes and is usually represented as a 3D array, the number of elements of which is $(l_1 + 1) \times (l_2 + 1) \times (l_3 + 1) = 31 \times 63 \times 20 = 39\,060$ for anharmonic oscillators. However, most of the elements in this array are zero due to the constraint $\varepsilon_{i_1,i_2,i_3} < D$. Storage of such an array and access to its elements require high computer performance in terms of memory. Moreover, nested loops over i_1, i_2, i_3 are used to calculate thermodynamic functions, which significantly increases the computational costs. Therefore, when numerically solving the system (2) and (3), we decided not to work with the 3D array for $\varepsilon_{i_1,i_2,i_3}$ and rearranged it to a linear vector containing only nonzero 7964 elements of the 3D array. Accordingly, all variables depending on the vibrational state were also presented in the form of vectors.

Simulations using the state-to-state approach described above require solving a set of 7965 ordinary differential equations (ODEs) for the populations of all allowed vibrational states. The code was written in the MATLAB environment, which has a huge functionality for working with vectors and matrices, as well as a library of programs for solving systems of differential equations. But the main challenge is not even in the ODE solution, but in the need to calculate a large number of rate coefficients for the energy transitions that occupy a significant amount of computer memory. A possible solution to the problem of multiple operations with large variables can be parallel computing and acceleration using the graphics processing units (GPUs).

III. MULTI-TEMPERATURE DESCRIPTION

Although the efficient numerical implementation of the state-to-state model allows one to carry out relatively fast 0-D simulations, its usage in the real-geometry flows is still challenging. Therefore, less computationally demanding models, such as multi-temperature approaches, are of great interest.

A. Three-temperature approach

In the present section, we consider a multi-temperature description of the problem for which the following relation of characteristic relaxation times holds:

$$\tau_{tr} < \tau_{\text{rot}} < \tau_{\text{VV}_m} \sim \tau_{\text{VV}_{1-2}} \ll \tau_{\text{VT}_2} \sim \tau_{\text{VV}_{2-3}} \sim \tau_{\text{VV}_{1-2-3}} \sim \theta, \quad m = 1, 2, 3, \tag{18}$$

where τ_γ is the characteristic time for the γ process. Note that VT_3 transitions are not included in the kinetic scheme since they are assumed to be frozen.

Taking into account the rapid VV_{1-2} and VV_m vibrational energy exchanges, the vibrational temperatures T_{12}, T_3 are introduced for the coupled (symmetric-bending) and asymmetric CO_2 modes, and vibrational level populations are written in the form of the three-temperature distribution [14]:

$$n_{i_1,i_2,i_3} = \frac{ns_{i_1,i_2,i_3}}{Z^{vibr}(T, T_{12}, T_3)} \exp\left[-\frac{\varepsilon_{i_1,i_2,i_3} - (i_1\varepsilon_{1,0,0} + i_2\varepsilon_{0,1,0} + i_3\varepsilon_{0,0,1})}{k_B T} - \frac{i_1\varepsilon_{1,0,0} + i_2\varepsilon_{0,1,0}}{k_B T_{12}} - \frac{i_3\varepsilon_{0,0,1}}{k_B T_3}\right], \tag{19}$$

where $s_{i_1,i_2,i_3} = i_2 + 1$ is the vibrational statistical weight, T_{12} is the vibrational temperature of the coupled (symmetric and bending) mode, T_3 is the vibrational temperature of the asymmetric mode, and Z^{vibr} is the corresponding vibrational partition function:

$$Z^{\text{vibr}}(T, T_{12}, T_3) = \sum_{i_1,i_2,i_3} s_{i_1,i_2,i_3} \exp\left[- \frac{\varepsilon_{i_1,i_2,i_3} - (i_1\varepsilon_{1,0,0} + i_2\varepsilon_{0,1,0} + i_3\varepsilon_{0,0,1})}{k_B T} \right.$$
$$\left. - \frac{i_1\varepsilon_{1,0,0} + i_2\varepsilon_{0,1,0}}{k_B T_{12}} - \frac{i_3\varepsilon_{0,0,1}}{k_B T_3} \right]. \tag{20}$$

Vibrational distribution (19) represents one of the extensions of the Treanor distribution [39], originally derived for diatomic molecules, to the case of CO_2 (see, also, [40–42] for various types of Treanor-like distributions in polyatomic gases). Under condition (18), fast VV_{1-2} exchange between symmetric and bending vibrations leads to the strong coupling of the corresponding modes and, as a consequence, to the adjustment of their temperatures. The asymmetric mode remains isolated in the fast processes and, therefore, has its own vibrational temperature. It is worth noting that similarly to diatomic species, the Treanor distribution is valid only for the states located below its minimum, and then yields unphysically increasing branches. However, the definition of the minimum for distribution (19) is a very complicated task due to the mode coupling and cannot be done analytically. Therefore, for the test cases showing the population inversion, we decided to use the harmonic oscillator model. In this case, the first terms in the exponential function in Eqs. (19) and (20) vanish, and the distribution is reduced to the Boltzmann one [14].

In the three-temperature approach for anharmonic oscillators, the fluid-dynamic variables associated with the vibrational relaxation are the numbers of vibrational quanta per unit mass associated with the quantum numbers $2i_1 + i_2$ and i_3 conserved in the fast processes [43],

$$\rho W_{12} = \sum_{i_1,i_2,i_3} (2i_1 + i_2) n_{i_1 i_2 i_3}(T, T_{12}, T_3), \tag{21}$$

$$\rho W_3 = \sum_{i_1,i_2,i_3} i_3 n_{i_1 i_2 i_3}(T, T_{12}, T_3). \tag{22}$$

The total energy in this case also depends on three temperatures through the specific vibrational energy defined by Eq. (6) and vibrational distribution (19).

The set of governing equations in the three-temperature approach includes the conservation equation of total energy (3) coupled to the relaxation equations for W_{12}, W_3,

$$\rho \frac{dW_{12}}{dt} = R_{12} = R_{12}^{\text{VT}_2} + R_{12}^{\text{VV}_{2-3}} + R_{12}^{\text{VV}_{1-2-3}}, \tag{23}$$

$$\rho \frac{dW_3}{dt} = R_3 = R_3^{\text{VT}_2} + R_3^{\text{VV}_{2-3}} + R_3^{\text{VV}_{1-2-3}}, \tag{24}$$

where the production terms are introduced for all slow processes indicated in Eq. (18).

The most self-consistent way to define R_{12}, R_3 is to average the state-resolved production terms substituting there vibrational distribution (19), multiplying by the corresponding invariant, and summing over vibrational states [16]. For instance,

$$R_{12}^{\text{VT}_2} = \sum_{i_1,i_2,i_3} (2i_1 + i_2) R_{i_1,i_2,i_3}^{\text{VT}_2}, \tag{25}$$

$$R_3^{\text{VT}_2} = \sum_{i_1,i_2,i_3} i_3 R_{i_1,i_2,i_3}^{\text{VT}_2}, \tag{26}$$

where $R_{i_1,i_2,i_3}^{\text{VT}_2}$ is specified by Eq. (8). The remaining production terms are introduced similarly on the basis of the state-specific terms (11) and (12).

This method is rigorous and rather natural and shows good results for diatomic species [44,45]. It is, however, extremely time consuming for polyatomic gases; applying it in real CO_2 flows may significantly increase computational efforts and thus cancel out the main advantage of the multi-temperature approach with respect to the state-to-state model, namely, its numerical efficiency. Averaged state-resolved production terms used in multi-temperature CO_2 flow simulations is an approach that we assess in the present study, among others.

Instead of using (25), (26), and similar expressions, simple approximate models based on the Landau-Teller formula are commonly applied [15,23]. The production terms rely on the experimentally measured relaxation times and have the form

$$R_{12}^{\gamma} = \rho \frac{W_{12}^{eq}(T) - W_{12}(T, T_{12})}{\tau_{\gamma}}, \tag{27}$$

$$R_{3}^{\gamma} = \rho \frac{W_{3}^{eq}(T) - W_{3}(T, T_{3})}{\tau_{\gamma}}, \tag{28}$$

where γ stands for VT_2, VV_{2-3}, VV_{1-2-3} processes, and W_{12}^{eq}, W_3^{eq} are equilibrium values of the corresponding numbers of quanta. In the present study, the characteristic relaxation times of the energy exchanges are calculated using the data of [30].

For harmonic oscillators, relaxation equations for the vibrational quanta (23) and (24) are reduced to the equations for the specific vibrational energy in CO_2 modes [14]. In this case, to describe VT_2 and VV_{2-3} vibrational transitions, the expressions given in [46] can also be used under several simplifying assumptions, in particular, an infinite harmonic oscillator, independent vibrational modes, imposed by the SSH theory relation between the transition probabilities, and weak deviations from equilibrium.

B. Two-temperature approach

In the case when fast processes include also intermode VV_{2-3} and VV_{1-2-3} transitions, relaxation proceeds through VT_2 transitions ($\tau_{VT_2} \sim \theta$, whereas all other processes are fast) and we can introduce a new collision invariant associated to all three modes, $(2i_1 + i_2 + 3i_3)$. Then the total specific number of vibrational quanta W could be written in the form

$$\rho W = \sum_{i_1, i_2, i_3} (2i_1 + i_2 + 3i_3) n_{i_1 i_2 i_3}(T, T_V), \tag{29}$$

as a function of the gas temperature T and the single vibrational temperature of the molecules T_V.

The set of governing equations in the two-temperature approach, instead of Eqs. (21) and (22), includes one equation for W,

$$\rho \frac{dW}{dt} = R^{VT_2}. \tag{30}$$

The right-hand side in Eq. (30) is commonly expressed using the Landau-Teller formula,

$$R^{VT_2} = \rho \frac{W^{eq}(T) - W(T, T_V)}{\tau_{VT_2}}. \tag{31}$$

For harmonic oscillators, the above equations are written for the total specific vibrational energy E_{vibr}.

IV. RESULTS AND DISCUSSION

A. Test case description

The simulations in pure CO_2 are carried out for a spatially homogeneous problem using three approaches. It is worth mentioning that for state-to-state modeling, the inclusion of intramode VV_m

transitions presents a great challenge. For example, the array with only values of rate coefficients $k_{i_1,i_1-1}^{k_1,k_1+1}$ for all states contains about 63.4 million elements and occupies approximately 500 MB of memory. This greatly complicates the calculations. Therefore, state-to-state simulations were first carried out neglecting the VV_m processes, and the estimation of their possible contribution was made *a posteriori* by calculating their contribution to the total vibrational energy variation on the basis of the obtained solution.

In the state-to-state simulations, several kinetic schemes are assessed using both harmonic and anharmonic oscillator models:

(1) [all processes] means that all single-quantum VT_m and multi-quantum VV_{1-2}, VV_{2-3}, VV_{1-2-3} transitions are included to the scheme.

(2) [only VT_m] transitions are included whereas the intermode VV exchange is neglected.

(3) [$VT_2 + VV_{2-3} + VT_{1-2-3}$]. This case was selected on the basis of processes that are taken into account in the three-temperature model.

(4) Moreover, in order to identify key relaxation mechanisms, we considered multiple test cases including successively different vibrational energy transitions. The total number of studied test cases is 16.

In the two-temperature approach, as noted earlier, only VT_2 transitions are taken into account.

Moreover, to study the effect of the number of the excited vibrational states on the temperatures and level populations, two reduced schemes are implemented along with the full scheme. Thus, three cases are studied:

(1) The full set of vibrational states up to the dissociation energy $D = 5.44$ eV.

(2) All vibrational states located below the energy threshold set to $D^* = 3$ eV; such a reduced model was proposed in [3] for simulations of the flow along the stagnation line.

(3) The set of vibrational levels proposed in [5], which includes the full vibrational ladder of the asymmetric mode (20 levels) and two lowest states in the symmetric and bending modes. Such a set of levels is now widely used in plasma chemistry applications for modeling CO_2 conversion.

For the reduced models, it is possible to implement intramode VV_m transitions and thus self-consistently assess their contributions.

As initial conditions, we take a pressure $p^{(0)} = 100$ Pa, and consider two cases corresponding to high-temperature shock heated flows and low-temperature expanding flows:

(i) $T^{(0)} = 5000$ K, $T_V^{(0)} = 1000$ K

(ii) $T^{(0)} = 300$ K, $T_V^{(0)} = 1500$ K.

The initial population of the vibrational levels is specified by the Boltzmann distribution with the vibrational temperature T_V.

The state-to-state calculations are performed using the anharmonic oscillator, unless otherwise indicated. It should be noted that the use of the multi-temperature approaches based on the anharmonic oscillator model in the case of an initially excited gas is limited due to the appearance of unphysically increasing branches in the vibrational distributions of molecules. In order to remove this restriction, we use the harmonic oscillator model, which simplifies the form of the multi-temperature distributions.

B. Full state-to-state model

First we discuss the full state-to-state model. It should be noted that when we say "full model" we mean that it includes all known mechanisms of vibrational relaxation and the whole set of vibrational states below the dissociation threshold, contrary to other reduced models neglecting VT_1 and VT_3 transitions and using selected vibrational states. On the other hand, there are a number of assumptions which are used for the numerical implementation of the full model. Below they are listed explicitly:

(a) Based on kinetic scaling (1), rovibrational coupling is not taken into account since the characteristic time of rotational relaxation is assumed to be fast compared to that of vibrational

relaxation. This assumption is justified for temperatures below 10 000 K [47]; our test cases consider much lower temperatures.

(b) The rigid rotor model is used for the CO_2 rotational mode. Since CO_2 is a linear molecule, its rotational energy is described similarly to that of diatomic molecules. Under moderate temperature conditions, nonrigidity does not considerably affect the thermodynamic properties [48].

(c) State-dependent rate coefficients for vibrational energy transitions are obtained by averaging the corresponding transition probabilities over equilibrium rotational distributions with the gas temperature. Such an assumption is valid for kinetic scaling (1).

(d) Both harmonic and anharmonic oscillator models are used in the state-to-state simulations.

(e) Rate coefficients of vibrational energy transitions are calculated using the SSH theory [31]. One of the limitations of the SSH theory is that only single-quantum intramode VT_m transitions are allowed. Although this model has many limitations, it provides the complete set of transition probabilities for the full state-to-state model. We expect that the main mechanisms of vibrational relaxation are not sensitive to the specific transition probability model, and the SSH model gives qualitatively correct estimates.

(f) Quasibound rotational states as well as electronically excited states are neglected, although they can affect the dissociation processes at high temperatures [2]. This assumption is justified for the present test cases since the maximum temperature is 5000 K, and dissociation is not taken into account.

Let us evaluate the contribution of various processes to the formation of vibrational distribution functions (VDFs) and temperature profiles. Vibrational distributions are presented in Figs. 1 and 2. In Fig. 1, the VDF in each CO_2 mode is plotted as a function of the vibrational energy calculated for the corresponding quantum number for different time points. The case [all processes] is considered; the quantum number of other modes is set to zero. For higher states of other modes, the results are qualitatively similar.

In general, the evolution of vibrational level populations in CO_2 molecules is rather complicated due to the competition of various processes. Nevertheless, the excitation and deactivation processes in the initially hot and cold gases, respectively, can be clearly observed. In the case $T^{(0)} > T_V^{(0)}$, initially the lower vibrational states are the most populated and their population decreases as a result of relaxation processes. Higher vibrational states at $t = 0$ are less populated and their number density increases with time. In the case $T^{(0)} < T_V^{(0)}$, the situation is opposite; one can see the depletion of high states with time. One can also notice that the behavior of different states populations can change both monotonically and nonmonotonically over time. It is interesting to note that whereas the VDFs in the symmetric mode look like the Boltzmann ones, in the other two modes, there are noticeable deviations, especially for the asymmetric mode distributions. The bending mode attains equilibrium faster than the stretching modes.

In Fig. 2, the VDFs are presented as functions of the vibrational energy, similarly to [3]. Three kinetic schemes are compared: the complete scheme, the scheme including only VT transitions, and the scheme used in the three-temperature model. It is worth mentioning that under thermal equilibrium conditions, the populations (the Boltzmann VDF) are localized around a straight line; thus, the VDFs corresponding to $t = 10^{-7}$ s in Fig. 2(a) and $t = 10^{-8}$ s in Fig. 2(b) are close to the Boltzmann ones. The nonequilibrium level populations are "spread" over a much wider range of values (for instance, at $t = 10^{-5}$ s). Thus one can notice that although the VDFs in the different modes look like the Boltzmann ones (see Fig. 1), the overall distributions are strongly non-Boltzmann. Comparing the VDFs, we see that under the considered conditions, the complete scheme [all processes] yields faster relaxation.

Let us now discuss the effect of the kinetic scheme on the temperature. In Table I, the maximum discrepancy in the temperature obtained for various schemes from that obtained in the [all processes] test case is presented. Neglecting intermode exchanges yields a considerable error for both the $T^{(0)} > T_V^{(0)}$ and $T^{(0)} < T_V^{(0)}$ cases. Including VT_3 transitions does not affect the accuracy; this process can be neglected in all cases. Including one of the VV_{2-3} or VV_{1-2-3} processes gives similar contributions; however, accounting simultaneously for both processes does not noticeably

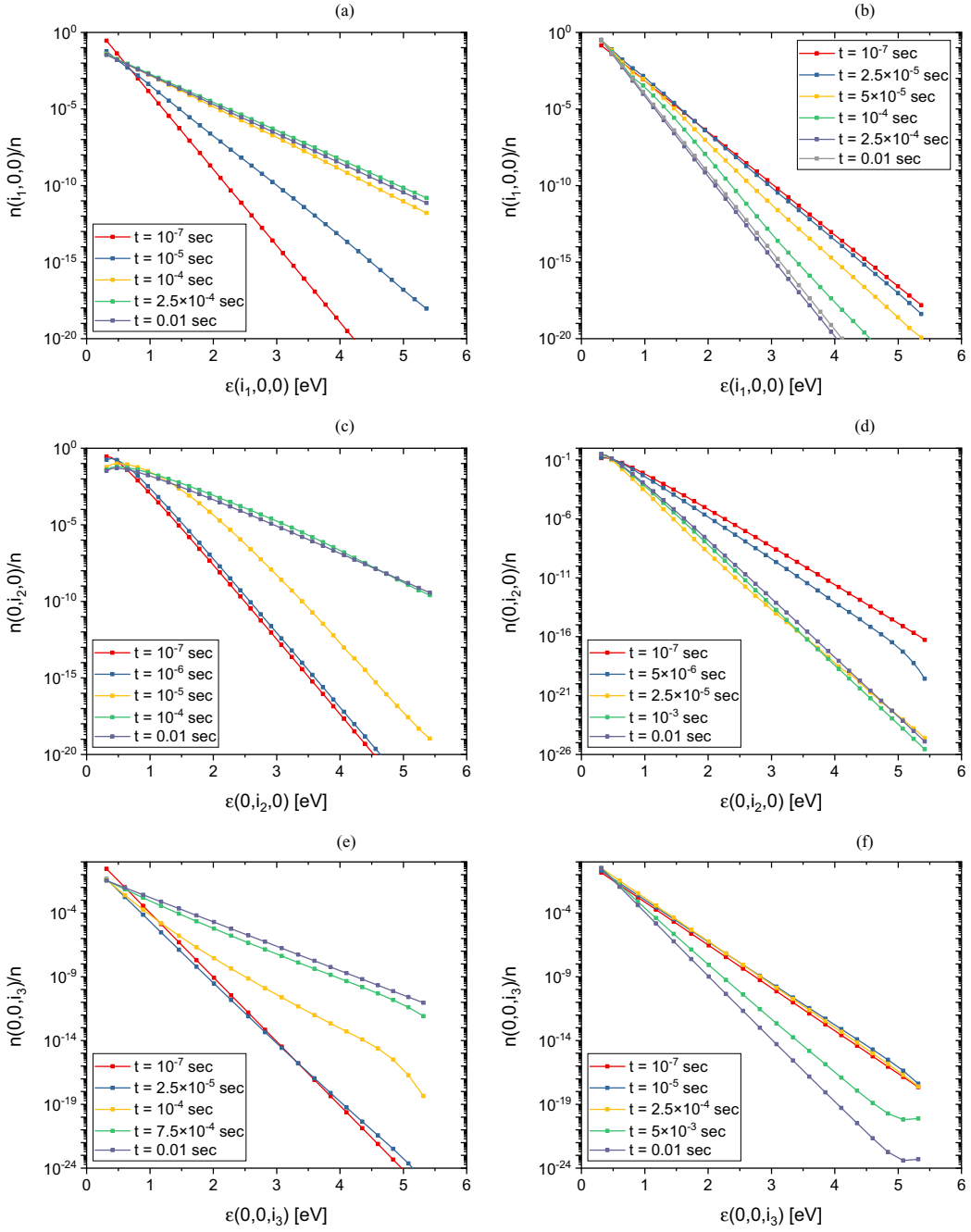

FIG. 1. Vibrational distributions of molecules in different modes vs vibrational energy for fixed moments of time. Case: [all processes]. Left: $T^{(0)} > T_V^{(0)}$; right: $T^{(0)} < T_V^{(0)}$.

improve the accuracy. Since calculation of their production terms R_{i_1,i_2,i_3} requires approximately the same number of operations and calls for the rate coefficients, we recommend to include VV_{2-3} transitions to the kinetic scheme for the case $T^{(0)} > T_V^{(0)}$ as it provides slightly better accuracy. It is

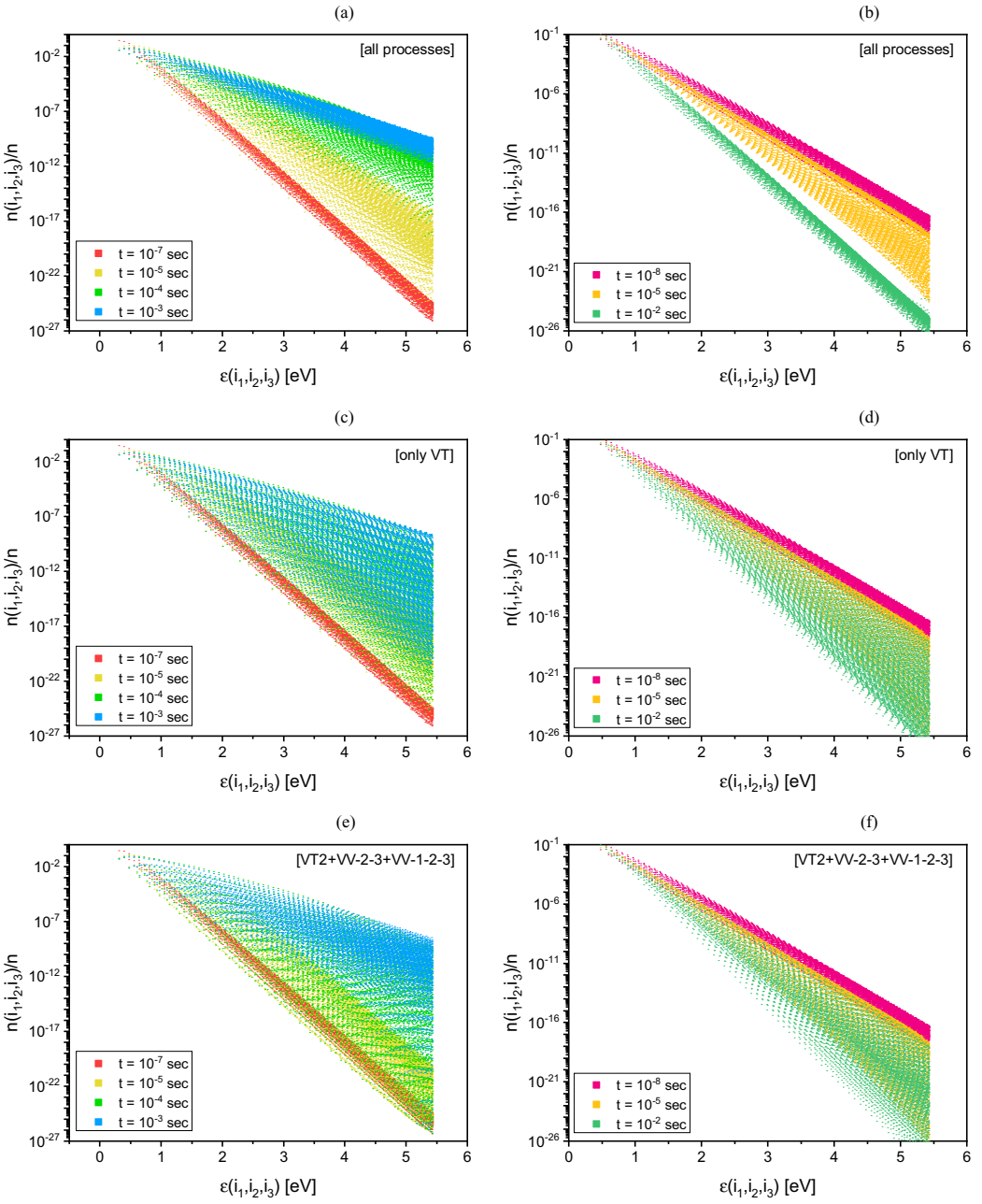

FIG. 2. Vibrational distributions of molecules vs vibrational energy for different moments of time. First row: [all processes]; second row: [only VT_m]; third row: [$VT_2 + VV_{2-3} + VT_{1-2-3}$]. Left column: $T^{(0)} > T_V^{(0)}$; right column: $T^{(0)} < T_V^{(0)}$.

interesting that for the hot gas ($T^{(0)} > T_V^{(0)}$), VT_1 transitions are more important than VV_{1-2}, and the numerically efficient scheme [$VT_1 + VT_2 + VV_{2-3}$] yields very good accuracy.

For the initially cold gas, neglecting VV_{1-2} transitions results in a considerable loss of accuracy, whereas VT_1 exchange does not affect it. A similar conclusion is drawn in [11] for a flow along the stagnation line, where the gas is cooling towards the surface. However, in [11], it is suggested to

TABLE I. Maximum temperature discrepancy (%) between [all processes] and other cases.

Cases	$T^{(0)} > T_V^{(0)}$	$T^{(0)} < T_V^{(0)}$
$[VT_1 + VT_2 + VT_3]$	7.89	9.99
$[VT_2 + VV_{2-3} + VV_{1-2-3}]$	13.13	14.04
$[VT_2 + VV_{1-2} + VV_{2-3} + VV_{1-2-3}]$	5.48	2.33×10^{-1}
$[VT_2 + VV_{1-2} + VV_{1-2-3}]$	5.61	4.91×10^{-1}
$[VT_1 + VT_2 + VV_{2-3}]$	2.73	9.93
$[VT_1 + VT_2 + VV_{1-2-3}]$	3.36	9.88
$[VT_1 + VT_2 + VT_3 + VV_{1-2}]$	7.91	5.96
$[VT_1 + VT_2 + VT_3 + VV_{2-3}]$	2.64	9.93
$[VT_1 + VT_2 + VT_3 + VV_{1-2-3}]$	3.25	9.88
$[VT_1 + VT_2 + VV_{1-2} + VV_{2-3}]$	2.29	3.67
$[VT_1 + VT_2 + VV_{1-2} + VV_{1-2-3}]$	1.94	4.89×10^{-1}
$[VT_1 + VT_2 + VV_{2-3} + VV_{1-2-3}]$	3.36	9.88
$[VT_1 + VT_2 + VT_3 + VV_{1-2} + VV_{2-3}]$	2.15	3.64
$[VT_1 + VT_2 + VT_3 + VV_{1-2} + VV_{1-2-3}]$	1.81	4.81×10^{-1}
$[VT_1 + VT_2 + VT_3 + VV_{2-3} + VV_{1-2-3}]$	2.25	9.83
$[VT_1 + VT_2 + VV_{1-2} + VV_{2-3} + VV_{1-2-3}]$	8.24×10^{-2}	6.56×10^{-3}

account for both VV_{1-2-3} and VV_{2-3} transitions. We think that the importance of the latter process was overestimated in [11] since the rate coefficients of this transition were calculated without the corrections mentioned above in Sec. II C. Thus, for the initially cold gas, we propose using the scheme $[VT_2 + VV_{1-2} + VV_{1-2-3}]$.

For the general case, when the flow regime is not known, we recommend the scheme $[VT_1 + VT_2 + VV_{1-2} + VV_{1-2-3}]$, which represents a good compromise in terms of accuracy and numerical efficiency. This scheme is highlighted in red in Table I.

In order to illustrate the effect of various energy exchanges on the relaxation process, we evaluate the contributions of each process to the total vibrational energy variation of the gas according to the following relation:

$$\Omega^{\gamma} = \sum_{i_1,i_2,i_3} R^{\gamma}_{i_1,i_2,i_3} \varepsilon_{i_1,i_2,i_3}. \tag{32}$$

It is worth noting that Ω^{γ} can change its sign during the relaxation. Thus, when plotting Ω^{γ}, we accept the following convention: if $\Omega^{\gamma} > 0$ in the whole range of time, we give its value directly; if $\Omega^{\gamma} < 0$ for all t, we plot $|\Omega^{\gamma}|$; if the sign is changing, we plot the logarithm function calculated as $\lg(\Omega) = \mathrm{sgn}(\Omega) \cdot [\lg(1+ \mid \Omega \mid)]$. For the latter case, the order of magnitude of Ω^{γ} is shown on the ordinate axis, and the plus or minus mark indicates its sign [see, for instance, Figs. 4(b) and 10(b)–10(d)].

The results of this evaluation are presented in Fig. 3 (Ω^{γ} for the initially hot gas and $|\Omega^{\gamma}|$ for the cold gas). One can see the dominating role of VT_2 transitions at the first relaxation stages; for the case $T^{(0)} > T_V^{(0)}$, VT_1 transitions are also important. With rising time, different contributions become closer and intermode exchanges start playing an important role.

Finally, we assess the possible contribution of intramode VV_m transitions. The estimates are based on the vibrational distributions and temperature obtained for the case [all processes]. The results are presented in Fig. 4 [Ω^{γ} for the initially hot gas and $\lg(\Omega^{\gamma})$ for the cold gas]. It can be seen that these processes may play a role if the gas is excited. Nevertheless, the contributions from the VV_m transitions are at least two orders of magnitude less than those from dominating processes. Therefore, the VV_m processes can be neglected in the state-to-state simulations, which greatly reduces the computational efforts.

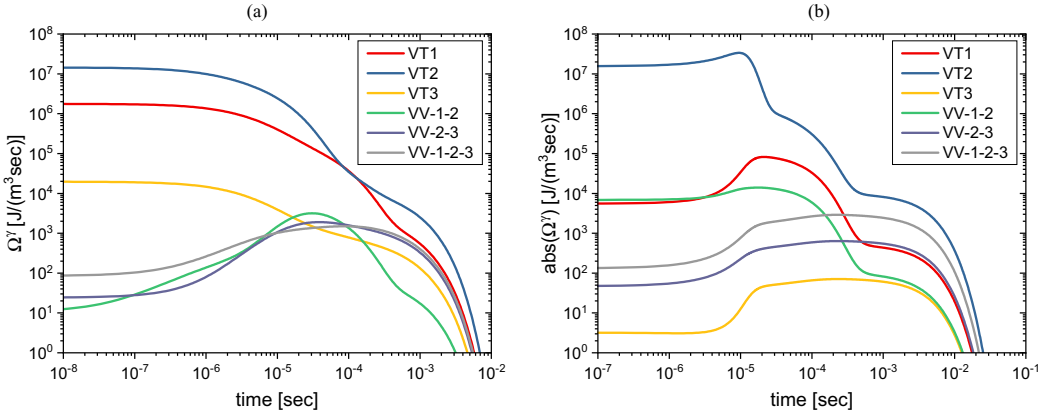

FIG. 3. Contributions of various processes to the total vibrational energy of a mixture vs time. Case: [all processes]. (a) Ω^γ; $T^{(0)} > T_V^{(0)}$. (b) $|\Omega^\gamma|$; $T^{(0)} < T_V^{(0)}$.

C. Comparison of STS and MT approaches

In this section, we compare the solutions obtained in the framework of the state-to-state (STS) and multi-temperature (MT) approaches. Time distributions of the gas temperature are presented in Fig. 5 for various approaches and kinetic schemes. From this point on, the symbols "a.o." and "h.o." refer to anharmonic and harmonic oscillators, respectively.

First, one can see that the two-temperature model fails to correctly describe the temperature evolution; it yields a very long incubation time compared to other models for both the $T^{(0)} > T_V^{(0)}$ and $T^{(0)} < T_V^{(0)}$ cases. Contrarily, the three-temperature (3T) approach shows much better results for the case of an initially hot gas [Fig. 5(a)]. At the early relaxation stage, the temperature profiles obtained within the STS and 3T models are rather close, but at $t \approx 10$ μs they start to diverge, and the temperature calculated using the 3T model attains equilibrium considerably faster. An attempt was made to keep in the STS simulation the same processes which are included to the 3T simulations, namely, [$\mathrm{VT}_2 + \mathrm{VV}_{2-3} + \mathrm{VV}_{1-2-3}$]. However, it gave a very different temperature profile and did not improve the agreement. Moreover, as is seen from Table I, this kinetic scheme is one of the worst among those considered and cannot be recommended for state-to-state simulations

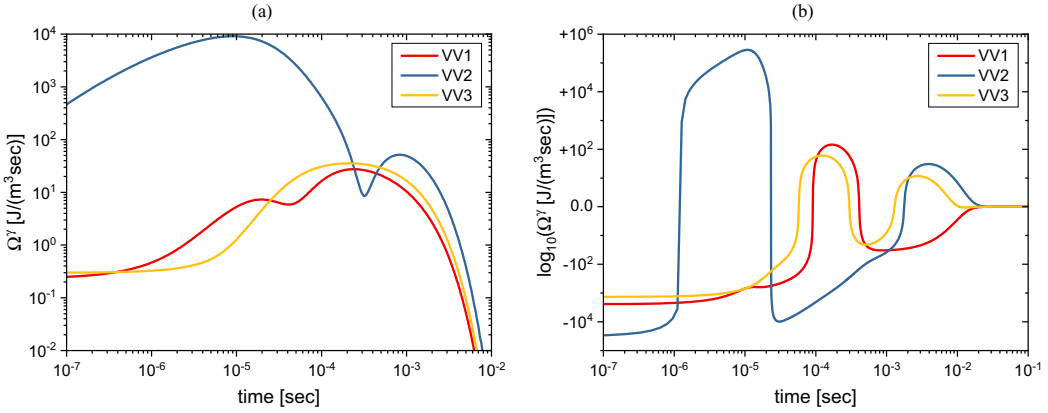

FIG. 4. Contributions of VV_m transitions to the total vibrational energy vs time. Case: [all processes]. (a) Ω^γ; $T^{(0)} > T_V^{(0)}$. (b) $\log_{10}(\Omega^\gamma)$; $T^{(0)} < T_V^{(0)}$.

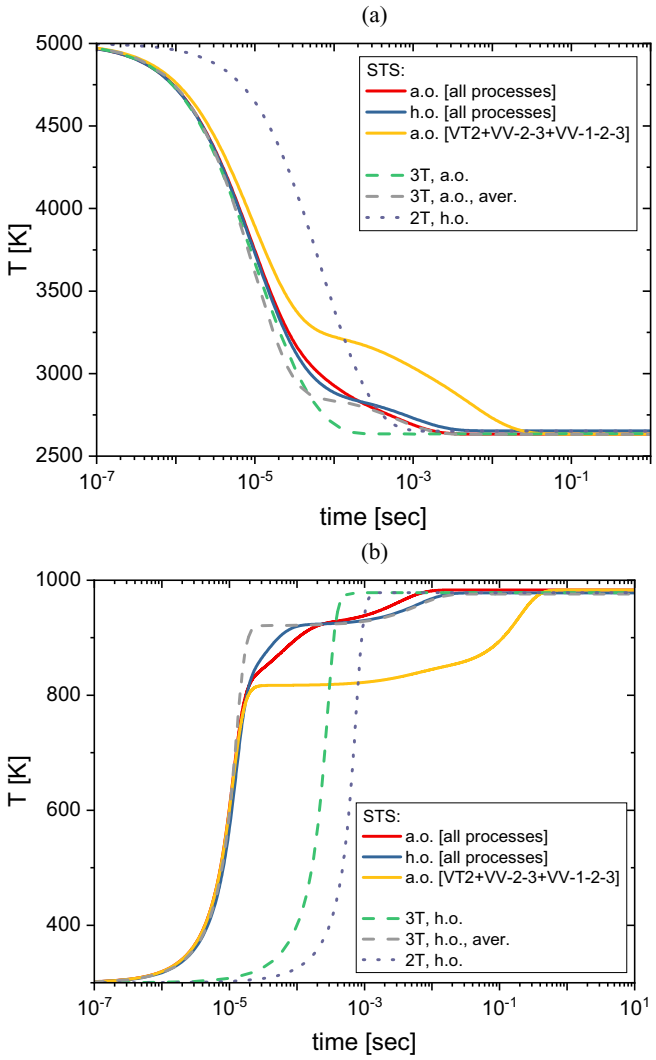

FIG. 5. Evolution of gas temperature. (a) $T^{(0)} > T_V^{(0)}$. (b) $T^{(0)} < T_V^{(0)}$.

of CO_2 flows. Based on Table I, one can suggest to improve the multi-temperature model including the VT_1 transitions; this means that the temperatures of the symmetric and bending modes have to be different. Such a four-temperature model was proposed in [43,49], but was never implemented in the CFD. Implementation of the four-temperature model is, however, beyond the scope of the present study.

Another source of discrepancy can be in using, in the 3T model, simplified production terms (27) and (28) instead of the rigorous ones (25) and (26). Thus, in [50,51], it was discussed that applying the Landau-Teller form for the intermode VV exchange may cause noticeable differences in the vibrational temperature profiles. Here we provide a systematic assessment of this assumption. For this purpose, we use in the 3T simulations the state-resolved production terms of the VT_2, VV_{2-3}, and VV_{1-2-3} processes averaged with quasistationary vibrational distributions (Treanor for anharmonic oscillators or Boltzmann for harmonic); the corresponding curve in Fig. 5 is denoted as "aver." One can see a considerable improvement of the solution at $t > 2 \times 10^{-4}$ s; the equilibrium is now attained at the same time. Yet, there is a discrepancy in the range 10^{-5}–10^{-4} s, which can be

attributed to the VT_1 and VV_{1-2} transitions which cannot be taken into account in the framework of the 3T model.

For the initially excited gas [Fig. 5(b)], both multi-temperature models fail to correctly describe the vibrational relaxation showing a very long incubation time and a sharp subsequent temperature increase. The kinetic scheme [$VT_2 + VV_{2-3} + VV_{1-2-3}$] also yields significant discrepancies. On the other hand, the effect of anharmonicity is rather weak and thus cannot explain the difference between the STS and 3T simulations. The failure of the original 3T model can be connected not only with the use of simplified production terms (27) and (28), but also with the fact that the relaxation times [30] measured in shock heated gases cannot properly describe the vibrational relaxation in the cooling regime. Using the averaged state-resolved production terms again significantly improves the solution; in this case, the temperature discrepancy between the STS and 3T models does not exceed 10–12%. This is especially noticeable when the 3T model is compared with the case STS h.o. where, with the exception of a small zone 10^{-5}–10^{-4} s, the temperature distributions completely coincide. The differences can be connected with VV_{1-2} exchanges not accounted for in the 3T model. It is interesting to note that for both STS and 3T simulations with the state-resolved production terms, one can see a kind of quasi-steady state (QSS) attained around $t \approx 10$ μs. The possible reasons are discussed later.

The change in the population of one selected vibrational state (we have chosen the state $i_1 = 1$, $i_2 = 8$, $i_3 = 1$, but similar conclusions are drawn for other states) is shown in Figs. 6(a) and 7(a) for the initially hot and cold gas, respectively. The corresponding production term $R_{1,8,1}$ calculated for the full STS model is presented in Figs. 6(b), 7(b), and 7(c). For the case of an initially hot gas (Fig. 6), the excitation proceeds monotonically; using the reduced scheme [$VT_2 + VV_{2-3} + VT_{1-2-3}$] yields a much slower excitation process. For the 2T model, one can notice a considerably longer incubation time, but faster equilibration. The final equilibrium state is a bit different due to the difference in the thermodynamic functions for harmonic and anharmonic oscillators. For the original 3T model, the relaxation starts earlier and the equilibrium is attained faster. However, if the averaged state-resolved production terms are used, then the evolution of the level populations is almost the same as for the full STS model. Analysis of the production term shows that in the beginning, the main relaxation mechanism is the VT_2 exchange in the bending mode and, to a lesser extent, in the symmetric mode. At times about 10 μs, the role of the VT processes decreases and the contribution of intermode VV exchange becomes important.

For the initially excited gas (Fig. 7), at $t < 10$ μs, the population decreases as a result of VT_2 and VV_{1-2} transitions; for $t > 10$ μs, its behavior is essentially nonmonotonic due to the competition of various processes. Both multi-temperature models yield monotonic evolution of this level population, long incubation time, and fast attaining of the final equilibrium state. When the state-resolved production terms are used in the 3T simulations, the evolution of $n(1, 8, 1)$ is close to that for the full STS h.o. model; the discrepancy around 10^{-5}–10^{-4} s is due to VV_{1-2} transitions. The effect of anharmonicity is noticeable for $t > 10$ μs; it also appears in the difference of the final equilibrium state.

As is mentioned above, for the initially cold gas, a kind of QSS is seen around 10^{-4}–10^{-3} s. It can be explained by the competition of VT_2 and VV_{1-2} processes which give similar contributions but act in the opposite directions [see Fig. 7(b)]. At this point, the role of the VV_{2-3} and VV_{1-2-3} transitions is still weak. With rising time, the contribution of the VV_{2-3} and VV_{1-2-3} exchange increases [see Fig. 7(c)] and destroys this quasiequilibrium. The final equilibrium is attained through the combination of all processes.

To conclude this section, we can say that multi-temperature models could provide an efficient alternative to the state-to-state models if the production terms in the relaxation equations are calculated correctly. Using the averaged state-resolved production terms is not numerically efficient since it needs computation and storage of all state-resolved rate coefficients. Therefore, derivation of the generalized Landau-Teller equations similar to those obtained for diatomic species [52,53] is rather promising for the improvement of the MT models. Another possible way to increase the

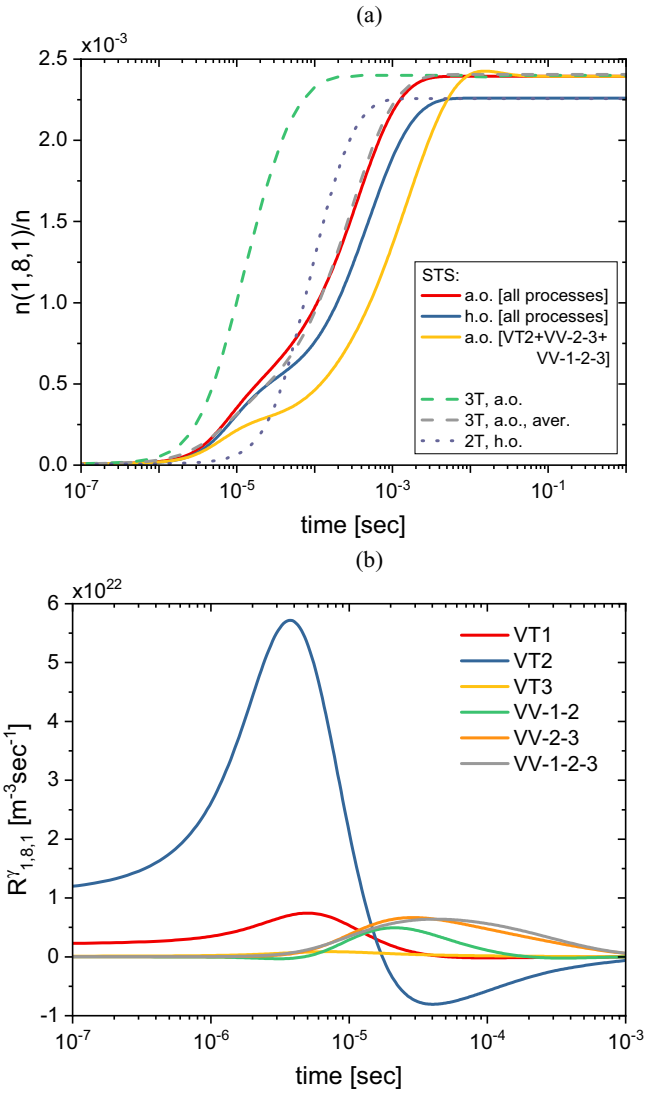

FIG. 6. (a) Evolution of the relative population of the state (1,8,1). (b) Relaxation terms $R^{\gamma}_{(1,8,1)}$ of different processes. Case: [all processes]; $T^{(0)} > T_V^{(0)}$.

accuracy while keeping the efficiency is to develop and implement the four-temperature model with different vibrational temperatures of all CO_2 modes.

D. Comparison with other reduced-order models

Another way to increase the efficiency of the state-to-state CO_2 flow simulations is to implement reduced STS models. One possibility is to keep the same structure of the vibrational levels but lower the threshold energy. In the present study, similarly to [3], we use the reduced model with the threshold energy of 3 eV instead of the dissociation energy $D = 5.44$ eV and take into account all the vibrational states located below. This reduces the number of states and corresponding master equations to 1177 and also significantly saves the computational efforts for calculation of the rate coefficients. The second possibility is to use some specific sets of levels as those proposed by Kozak

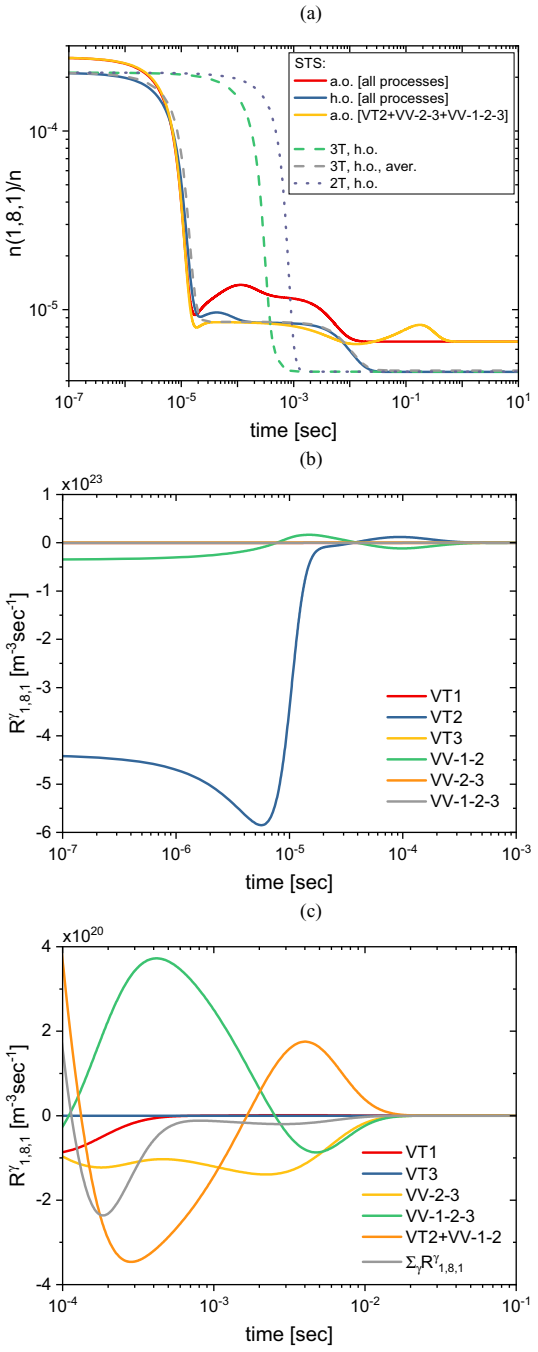

FIG. 7. (a) Evolution of the relative population of the state (1,8,1). (b) Relaxation terms $R^{\gamma}_{(1,8,1)}$ of different processes. (c) Relaxation terms $R^{\gamma}_{(1,8,1)}$ for $t > 10^{-4}$ s in an enlarged scale. Case: [all processes]. $T^{(0)} < T_V^{(0)}$.

and Bogaerts [5]. In that study, based on the Fridman model [2], the CO_2 molecule is assumed to have only a few vibrational states: all levels i_3 of the vibrational asymmetric mode at fixed $i_1 = i_2 = 0$, the levels $i_2 = 0 - 4$ of the bending mode at fixed $i_1 = i_3 = 0$, and states $(1, 0, 0) + (1, 1, 0) + (1, 2, 0) + (2, 0, 0)$. Thus this spectrum contains 28 vibrational states but excludes VV_{2-3} energy

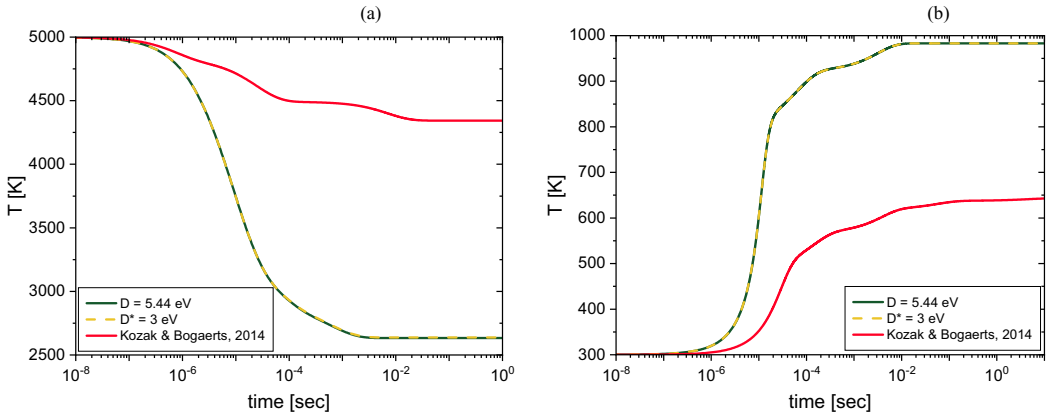

FIG. 8. Comparison of temperature evolution for different sets of vibrational levels. Case: [all processes]. (a) $T^{(0)} > T_V^{(0)}$. (b) $T^{(0)} < T_V^{(0)}$.

transitions. For both reduced-order models, we implement the full kinetic scheme. Moreover, due to the reduction of the computational complexity, it is also possible to include the intramode VV_m transitions to the kinetic scheme.

Figure 8 presents the temperature evolution for the full and reduced STS models; both $T^{(0)} > T_V^{(0)}$ and $T^{(0)} < T_V^{(0)}$ test cases are considered. One can see that the solutions obtained for the energy ladders limited at 5.44 and 3 eV coincide. Therefore, in the absence of dissociation, this model can be recommended for simulations. Moreover, including VV_m transitions to the kinetic scheme does not affect the temperature. This justifies that intramode VV exchange can be neglected in the kinetics, which drastically saves on the computational efforts. On the other hand, using the set of levels proposed in [5] yields different values of the equilibrium temperature. This is clear since the thermodynamic functions (in particular, the vibrational energy per unit mass) specified by such a reduced vibrational spectrum differ significantly from the real ones. This limits the range of applicability of the model [5] by the ambient temperatures and small departures from equilibrium, when the thermodynamic functions can be calculated using a few lowest states.

In Fig. 9, the vibrational distributions obtained using the reduced-order models are compared. It is interesting that the general trends are similar for both models; the rates of the excitation process

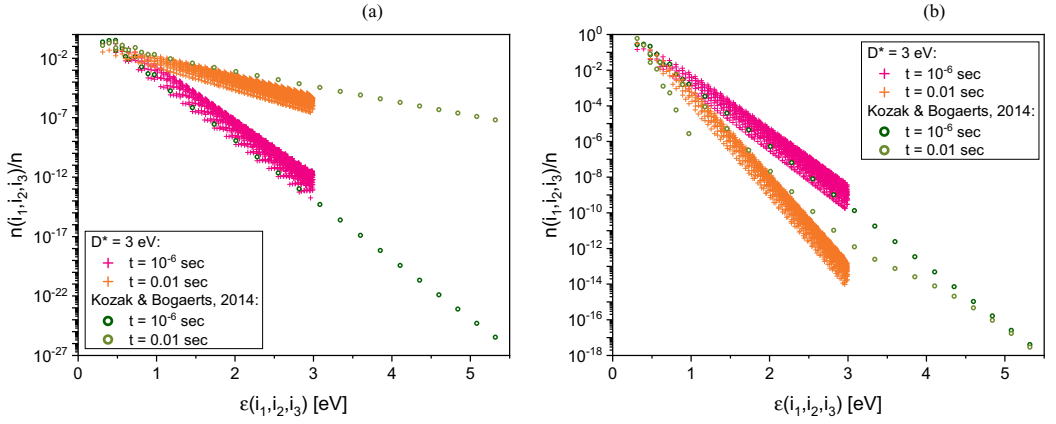

FIG. 9. Vibrational distributions of molecules vs vibrational energy for different sets of vibrational levels. Case: [all processes]+$\mathrm{VV}_1 + \mathrm{VV}_2 + \mathrm{VV}_3$. (a) $T^{(0)} > T_V^{(0)}$; (b) $T^{(0)} < T_V^{(0)}$.

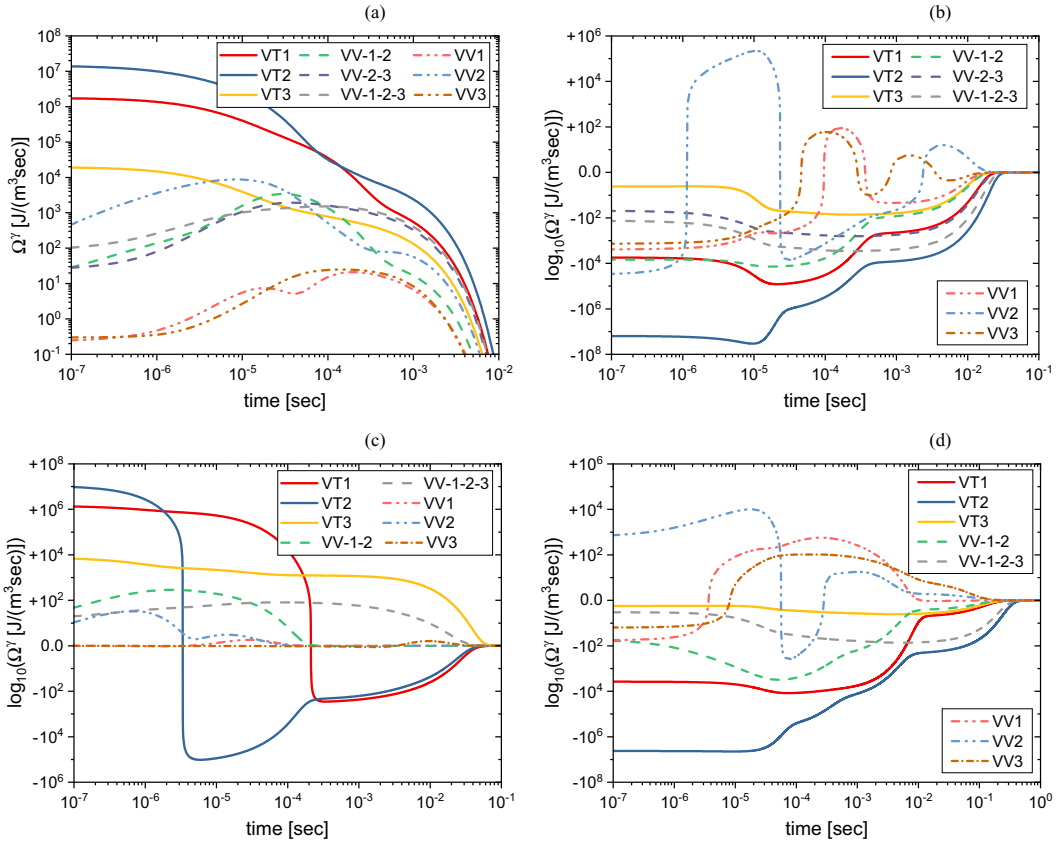

FIG. 10. Contributions of various processes to the total vibrational energy vs time. Case: [all processes]+$VV_1 + VV_2 + VV_3$. Top row: case $D^* = 3$ eV; bottom row: vibrational ladder from Ref. [5]. (a) Ω^γ; (b)–(d) $\log_{10}(\Omega^\gamma)$. Left column: $T^{(0)} > T_V^{(0)}$; right column: $T^{(0)} < T_V^{(0)}$.

[Fig. 9(a)] are comparable. In the case of the deactivation relaxation mechanism [Fig. 9(b)], the VDF obtained at $t = 0.01$ s using the model [5] shows a non-Boltzmann shape, with overpopulated high vibrational states. This is, perhaps, a justification for the assumption about vibrationally enhanced dissociation, which is the basic idea of studies [5,54]. However, one has to be careful since the full STS model does not yield such high populations in the asymmetric mode at the same time point; see Fig. 1(f). This can be explained by the fact that changing the set of accounted vibrational states affects the contribution of various processes to the total vibrational energy; see Fig. 10. For the excitation mode ($T^{(0)} > T_V^{(0)}$), STS simulations accounting for all vibrational states below 3 eV yield positive values of Ω^γ. For the model proposed in Ref. [5], the contributions of the VT transitions change their signs with time. For the deactivation mode ($T^{(0)} < T_V^{(0)}$), the trends are more or less similar but shifted in time. Therefore, we conclude that using selected sets of levels with the same kinetic scheme may considerably affect the temperature evolution and vibrational distributions.

V. CONCLUSIONS

Space homogeneous vibrational relaxation in the single-component CO_2 gas was studied using full and reduced state-to-state models and several multi-temperature approaches. The full model includes about 8000 vibrational states and all possible VT and intermode VV transitions. Two

generic test cases were considered, with initially hot and cold gases, corresponding to compression flows (excitation regime) and expanding flows (deactivation regime). For both cases, dominating processes were identified and kinetic schemes combining acceptable accuracy and numerical efficiency were proposed. For the excitation regime, the main role belongs to VT_1, VT_2, and VV_{2-3} transitions; for the deactivation mode, the best description is given by the scheme including VT_2, VT_{1-2}, and VV_{1-2-3} exchanges. For an arbitrary flow regime, we recommend a bit more expensive but general model, $[VT_1 + VT_2 + VV_{1-2} + VV_{1-2-3}]$. The contribution of intramode VV_m transitions and VT_3 exchange in the asymmetric mode to the time distributions of temperature and specific vibrational energy is found to be negligible.

Solutions obtained in the framework of the state-to-state approach were compared to the results of various multi-temperature simulations, and the main sources of discrepancy were detected. The two-temperature model assuming rapid intermode vibrational energy exchanges and a single vibrational temperature of all CO_2 modes cannot be applied at any relaxation stage; its accuracy is rather low. The original three-temperature model based on the experimentally measured relaxation times provides an acceptable agreement for the temperature distribution in the hot gas for an early relaxation stage; with rising time, the discrepancy occurs. For the cold gas, this model does not work, which can be explained by the fact that the relaxation times measured in shock heated gases fail to describe the cooling regime. However, if the averaged state-resolved production terms are used in the three-temperature model instead of the Landau-Teller relaxation terms, the agreement with the state-to-state model is fairly good for both test cases. This is the main result of the comparisons showing a coherence of state-to-state and multi-temperature approaches, if the energy production terms are calculated in a self-consistent way. Nevertheless, such a technique, although providing good accuracy, requires significant computational efforts and thus destroys the main advantage of the MT model, i.e., its numerical efficiency.

Based on the analysis performed in this study, we see several ways to improve the multi-temperature models: development of the generalized Landau-Teller formulas suitable for polyatomic gases with intermode vibrational energy exchange, modification of the multi-temperature model introducing different temperatures of symmetric and bending modes which allows inclusion of VT_1 and VV_{1-2} transitions to the kinetics, and development of rigorous theoretical models for the relaxation times, independent of the considered temperature range. Such models may be derived using the kinetic theory methods if information on the cross sections of various vibrational energy transitions is available.

Finally, two reduced state-to-state models were assessed. It is shown that in the absence of dissociation, lowering the threshold energy to 3 eV does not affect the solution if all vibrational states below this energy are taken into account. This allows for considerable reduction of the computational efforts. Contrarily, the model based on the set of selected states cannot be applied for high-temperature regimes, and can be used only at ambient temperatures when the excitation of symmetric and bending vibrations has no effect on the thermodynamic functions.

In our future studies, we plan to include state-resolved chemical reactions consistently coupled to vibrational energy exchanges in order to study relaxation mechanisms under high-temperature conditions.

ACKNOWLEDGMENT

This study was supported by the Russian Science Foundation (Project No. 19-11-00041).

[1] E. V. Kustova and E. A. Nagnibeda, State-to-state theory of vibrational kinetics and dissociation in three-atomic gases, *AIP Conference Proceedings*, Vol. 585, edited by T. J. Bartel and M. A. Gallis (American Institute of Physics, Melville, NY, 2001), pp. 620–627.

[2] A. Fridman, *Plasma Chemistry* (Cambridge University Press, New York, 2008).

[3] I. Armenise and E. Kustova, State-to-state models for CO_2 molecules: From the theory to an application to hypersonic boundary layers, Chem. Phys. **415**, 269 (2013).
[4] I. Armenise and E. Kustova, On different contributions to the heat flux and diffusion in non-equilibrium flows, Chem. Phys. **428**, 90 (2014).
[5] T. Kozak and A. Bogaerts, Splitting of CO_2 by vibrational excitation in non-equilibrium plasmas: A reaction kinetics model, Plasma Sources Sci. Technol. **23**, 045004 (2014).
[6] A. Bogaerts, W. Wang, A. Berthelot, and V. Guerra, Modeling plasma-based CO_2 conversion: Crucial role of the dissociation cross section, Plasma Sources Sci. Technol. **25**, 055016 (2016).
[7] L. D. Pietanza, G. Colonna, V. Laporta, R. Celiberto, G. D'Ammando, A. Laricchiuta, and M. Capitelli, Influence of electron molecule resonant vibrational collisions over the symmetric mode and direct excitation-dissociation cross sections of CO_2 on the electron energy distribution function and dissociation mechanisms in cold pure CO_2 plasmas, J. Phys. Chem. A **120**, 2614 (2016).
[8] L. D. Pietanza, G. Colonna, G. D'Ammando, and M. Capitelli, Time-dependent coupling of electron energy distribution function, vibrational kinetics of the asymmetric mode of CO_2 and dissociation, ionization and electronic excitation kinetics under discharge and post-discharge conditions, Plasma Phys. Controlled Fusion **59**, 014035 (2017).
[9] T. Silva, M. Grofulović, B. L. M. Klarenaar, A. S. Morillo-Candas, O. Guaitella, R. Engeln, C. D. Pintassilgo, and V. Guerra, Kinetic study of low-temperature CO_2 plasmas under non-equilibrium conditions. I. Relaxation of vibrational energy, Plasma Sources Sci. Technol. **27**, 015019 (2018).
[10] P. Diomede, M. C. M. van de Sanden, and S. Longo, Insight into CO_2 dissociation in plasmas from numerical solution of a vibrational diffusion equation, J. Phys. Chem. C **121**, 19568 (2017).
[11] I. Armenise and E. Kustova, Mechanisms of coupled vibrational relaxation and dissociation in carbon dioxide, J. Phys. Chem. A **122**, 5107 (2018).
[12] I. Armenise and E. Kustova, Effect of asymmetric mode on CO_2 state-to-state vibrational-chemical kinetics, J. Phys. Chem. A **122**, 8709 (2018).
[13] C. Park, J. T. Howe, R. L. Howe, R. L. Jaffe, and G. V. Candler, Review of chemical-kinetic problems of future NASA missions, II: Mars entries, J. Thermophys. Heat Transfer **8**, 9 (1994).
[14] E. V. Kustova and E. A. Nagnibeda, On a correct description of a multi-temperature dissociating CO_2 flow, Chem. Phys. **321**, 293 (2006).
[15] E. V. Kustova, E. A. Nagnibeda, Yu. D. Shevelev, and N. G. Syzranova, Different models for CO_2 flows in a shock layer, Shock Waves **21**, 273 (2011).
[16] E. V. Kustova and E. A. Nagnibeda, Kinetic model for multi-temperature flows of reacting carbon dioxide mixture, Chem. Phys. **398**, 111 (2012).
[17] I. Armenise, P. Reynier, and E. Kustova, Advanced models for vibrational and chemical kinetics applied to Mars entry aerothermodynamics, J. Thermophys. Heat Transfer **30**, 705 (2016).
[18] E. Kustova, M. Mekhonoshina, and A. Kosareva, Relaxation processes in carbon dioxide, Phys. Fluids **31**, 046104 (2019).
[19] A. Sahai, B. E. Lopez, C. O. Johnston, and M. Panesi, Adaptive coarse graining method for energy transfer and dissociation kinetics of polyatomic species, J. Chem. Phys. **147**, 054107 (2017).
[20] V. I. Gorikhovsky and E. A. Nagnibeda, Energy exchange rate coefficients in modeling carbon dioxide kinetics: Calculation optimization, Vestnik St. Petersb. Univ. Math. **52**, 428 (2019).
[21] A. Sahai, C. O. Johnston and B. Lopez, and M. Panesi, Flow-radiation coupling in CO_2 hypersonic wakes using reduced-order non-Boltzmann models, Phys. Rev. Fluids **4**, 093401 (2019).
[22] A. Kosareva and E. Nagnibeda, Vibrational-chemical coupling in mixtures CO_2/CO/O and CO_2/CO/O_2/O/C, J. Phys.: Conf. Ser. **815**, 012027 (2017).
[23] A. Kosareva and G. Shoev, Numerical simulation of a CO_2, CO, O_2, O, C mixture: Validation through comparisons with results obtained in a ground-based facility and thermochemical effects, Acta Astronaut. **160**, 461 (2019).
[24] B. R. Hollis and J. N. Perkins, Hypervelocity aeroheating measurements in wake of Mars mission entry vehicle, AIAA Paper 95-2314 (1995), doi:10.2514/6.1995-2314.
[25] B. R. Hollis and J. N. Perkins, High-enthalpy aerothermodynamics of a Mars entry vehicle. Part 1: Experimental results, J. Spacecr. Rockets **34**, 449 (1997).

[26] G. Herzberg, *Infrared and Raman Spectra of Polyatomic Molecules*, (D. Van Nostrand, New York, 1951).
[27] R. L. Taylor and S. Bitterman, Survey of vibrational relaxation data for process important in the CO_2-N_2 laser system, Rev. Mod. Phys. **41**, 26 (1969).
[28] J. A. Blauer and G. R. Nickerson, A survey of vibrational relaxation rate data for processes important to CO_2-N_2-H_2O infrared plume radiation, AFRPL-TR-73-57, Air Force Rocket Propulsion Laboratory, Director of Science and Technology, Air Force Systems Command: Edwards, CA, 1973.
[29] O. V. Achasov and D. S. Ragosin, Rate constants of V-V exchange for CO_2-GDL, Preprint No. 16, (Institute of Heat and Mass Transfer, Minsk, Bielarus, 1986).
[30] S. Losev, P. Kozlov, L. Kuznezova, V. Makarov, Yu. Romanenko, S. Surzhikov, and G. Zalogin, Radiation of CO_2-N_2-Ar mixture in a shock wave: Experiment and modeling, in *Proceedings of 3rd European Symposium on Aerothermodynamics for Space Vehicles*, Vol. 426 (ESTEC, Noordwiik, 1998), pp. 437-444.
[31] R. N. Schwartz, Z. I. Slawsky, and K. F. Herzfeld, Calculation of vibrational relaxation times in gases, J. Chem. Phys. **20**, 1591 (1952).
[32] C. T. Wickham-Jones, C. J. S. M. Simpson, and D. C. Clary, Experimental and theoretical determination of rate constants for vibrational relaxation of CO_2 and CH_3F by He, Chem. Phys. **117**, 9 (1987).
[33] M. Bartolomei, F. Pirani, A. Laganà, and A. Lombardi, A full dimensional grid empowered simulation of the $CO_2 + CO_2$ processes, J. Comput. Chem. **33**, 1806 (2012).
[34] A. Lombardi, N. Faginas-Lago, L. Pacifici, and G. Grossi, Energy transfer upon collision of selectively excited CO_2 molecules: State-to-state cross sections and probabilities for modeling of atmospheres and gaseous flows, J. Chem. Phys. **143**, 034307 (2015).
[35] I. V. Adamovich, S. O. Macheret, J. W. Rich, and C. E. Treanor, Vibrational energy transfer rates using a forced harmonic oscillator model, J. Thermophys. Heat Transfer **12**, 57 (1998).
[36] M. Lino da Silva, J. Vargas, and J. Loureiro, STELLAR CO2 v2: A database for vibrationally specific excitation and dissociation rates for carbon dioxide, Tech. Rep. No. IST–IPFN TR 06–2018 (IST, Lisbon, 2018).
[37] E. Kustova, A. Savelev, and I. Armenise, State-resolved dissociation and exchange reactions in CO_2 flows, J. Phys. Chem. A **123**, 10529 (2019).
[38] W. J. Witteman, Vibrational relaxation in carbon dioxide, J. Chem. Phys. **35**, 1 (1961).
[39] C. E. Treanor, I. W. Rich, and R. G. Rehm, Vibrational relaxation of anharmonic oscillators with exchange dominated collisions, J. Chem. Phys. **48**, 1798 (1968).
[40] A. A. Likalter, On the vibrational distribution of polyatomic molecules, Prikl. Mekh. Tekn. Fiz. **4**, 3 (1976).
[41] A. Cenian, Study of nonequilibrium vibrational relaxation of CO_2 molecules during adiabatic expansion in a supersonic nozzle. The Treanor distribution—existence and generation, Chem. Phys. **132**, 41 (1989).
[42] A. Chikhaoui and E. V. Kustova, Effect of strong excitation of CO_2 asymmetric mode on transport properties, Chem. Phys. **216**, 297 (1997).
[43] E. V. Kustova and E. A. Nagnibeda, Nonequilibrium distributions in CO_2 and their influence on the transport and thermodynamic properties, in *Rarefied Gas Dynamics 21*, Vol. 2, edited by R. Brun, R. Campargue, R. Gatignol, and J.-C. Lengrand (CEPADUES, Toulouse, France, 1999), pp. 289–296.
[44] I. N. Kadochnikov, B. I. Loukhovitski, and A. M. Starik, A modified model of mode approximation for nitrogen plasma based on the state-to-state approach, Plasma Sources Sci. Technol. **24**, 055008 (2015).
[45] E. Kustova, E. Nagnibeda, G. Oblapenko, A. Savelev, and I. Sharafutdinov, Advanced models for vibrational-chemical coupling in multi-temperature flows, Chem. Phys. **464**, 1 (2016).
[46] K. Maeno, A note of vibrational rate equations for CO_2-N_2 system applied to CO_2 gas dynamic laser, Memoirs Muroran Inst. Tech. **10**, 555 (1982).
[47] J. G. Kim and I. D. Boyd, State-resolved master equation analysis of thermochemical nonequilibrium of nitrogen, Chem. Phys. **415**, 237 (2013).
[48] E. Kustova, M. Mekhonoshina, and G. Oblapenko, On the applicability of simplified state-to-state models of transport coefficients, Chem. Phys. Lett. **686**, 161 (2017).
[49] E. V. Kustova and L. A. Puzyreva, Heat capacity of oscillatory-nonequilibrium carbon oxide gas, Vestnik Sankt-Peterburgskogo Universiteta. Ser 1., Math. Mech. Astron. **1**, 87 (2005).

[50] M. A. Abbasov, A. M. Kozhapenko, E. V. Kustova, L. A. Puzyreva, and A. Chikhaoui, Self-consistent and simplified descriptions of vibrational non-equilibrium CO_2 flows, AIP Conf. Proc. **1084**, 837 (2008).
[51] E. Kustova and M. Mekhonoshina, Multi-temperature vibrational energy relaxation rates in CO_2, Phys. Fluids **32**, 096101 (2020).
[52] E. Kustova and G. Oblapenko, Reaction and internal energy relaxation rates in viscous thermochemically non-equilibrium gas flows, Phys. Fluids **27**, 016102 (2015).
[53] E. Kustova and G. Oblapenko, Mutual effect of vibrational relaxation and chemical reactions in viscous multitemperature flows, Phys. Rev. E **93**, 033127 (2016).
[54] R. Aerts, T. Martens, and A. Bogaerts, Influence of vibrational states on CO_2 splitting by dielectric barrier discharges, J. Phys. Chem. C **116**, 23257 (2012).